

Energy scan/dependence of kinetic freeze-out scenarios of multi-strange and other identified particles in central nucleus-nucleus collisions

Muhammad Waqas^{1,2,3,*}, Fu-Hu Liu^{1,2,†}, Rui-Qin Wang^{4,‡}, Irfan Siddique^{5,§}

¹*Institute of Theoretical Physics & State Key Laboratory of Quantum Optics and Quantum Optics Devices, Shanxi University, Taiyuan, Shanxi 030006, People's Republic of China*

²*Collaborative Innovation Center of Extreme Optics, Shanxi University, Taiyuan, Shanxi 030006, People's Republic of China*

³*School of Nuclear Science and Technology, University of Chinese Academy of Sciences, Beijing 100049, People's Republic of China*

⁴*Department of Physics, Qufu Normal University, Qufu, Shandong 273165, People's Republic of China*

⁵*Department of Modern Physics, University of Science and Technology of China, Hefei, Anhui 230026, People's Republic of China*

Abstract: The transverse momentum (mass) spectra of the multi-strange and non-multi-strange (i.e. other identified) particles in central gold-gold (Au-Au), lead-lead (Pb-Pb), argon-muriate (Ar-KCl) and nickel-nickel (Ni-Ni) collisions over a wide energy range have been studied in this work. The experimental data measured by various collaborations have been analyzed. The blast-wave fit with Tsallis statistics is used to extract the kinetic freeze-out temperature and transverse flow velocity from the experimental data of transverse momentum (mass) spectra. The extracted parameters increase with the increase of collision energy and appear with the trend of saturation at the Beam Energy Scan (BES) energies at the Relativistic Heavy Ion Collider (RHIC). This saturation implies that the onset energy of phase transition of partial deconfinement is 7.7 GeV and that of whole deconfinement is 39 GeV. Furthermore, the energy scan/dependence of kinetic freeze-out scenarios are observed for the multi-strange and other identified particles, though the multiple freeze-out scenarios are also observed for various particles.

Keywords: Kinetic freeze-out temperature, transverse flow velocity, onset energy of phase transition, kinetic freeze-out scenario

PACS: 12.40.Ee, 13.85.Hd, 25.75.Ag, 25.75.Dw, 24.10.Pa

1 Introduction

High energy heavy ion collisions at the Relativistic Heavy Ion Collider (RHIC) in the Beam Energy Scan (BES) program offer a unique possibility to explore the quantum chromodynamics (QCD) phase diagram [1, 2, 3, 4]. The usual phase diagram of QCD is plotted as the chemical freeze-out temperature (T_{ch}) versus baryon chemical potential μ_B . Let us assume a thermalized system which is created in heavy ion collisions, T_{ch} and μ_B are expected to be varied with changing the collision energy [5, 6, 7]. Theories suggest the formation of QCD phase diagram which includes a possible transition from a high density and high temperature

phase known as quark-gluon plasma (QGP) phase and this phase has been predicted by the lattice QCD [8].

Lattice QCD calculations indicate the evolution of a rapid cross-over at the hadron to parton phase transition [9, 10] in the system at $\mu_B = 0$. Several QCD-based models [11, 12, 13, 14] and the calculations from lattice QCD [11] suggest the first order phase transition if the system created in collisions correspond to larger values of μ_B . The point in QCD phase diagram plane where the first order phase transition ends, is known as the QCD critical point [15, 16].

Experimental and theoretical nuclear physics research is currently focused on the digging out of critical

*E-mail: waqas_phy313@yahoo.com

†Corresponding author. E-mail: fuhuliu@163.com; fuhuliu@sxu.edu.cn

‡E-mail: wangrq@qfnu.edu.cn

§E-mail: irfans@mail.ustc.edu.cn

point and the phase boundary in the QCD phase diagram. The RHIC has undertaken the first phase of the BES program [17, 18, 19, 20, 21] upto this end, by varying the collision energy from the top RHIC to the lower most possible energy in order to look for the signatures of QCD phase boundary.

However, before looking to these signatures, it is very important to know the $T_{ch}-\mu_B$ region of the phase diagram we can access at the chemical freeze-out, as well as the kinetic freeze-out temperature T_0 or T_{kin} and transverse flow velocity β_T at the thermal and kinetic freeze-out. The transverse momentum (p_T) or mass (m_T) distributions of the particles and their yields are the tool to study the thermal and collective properties of the dense and hot hadronic matter formed in high energy collisions and it allows us to infer the related parameters at the kinetic and chemical freeze-outs.

In general, the freeze-out itself may be a complicated process, as it involves the duration in time, and a hierarchy where different types of particles and different reactions switch off at different times. According to the general kinematic arguments, it is expected that the reactions with the lower collision frequency then lower total cross-section switches off at higher densities/temperatures. However, the one with larger collision frequency and then larger total cross-section lasts longer. Therefore, the elastic cross-section is larger than inelastic cross-section in most cases, so the earlier occurrence of the inelastic (chemical) freeze-out than the elastic (kinetic) freeze-out is expected to happen. Generally, $T_{ch} > T_0$ according to the early study on this topic in ref. [22].

Furthermore, it is understood that the temperature is surely one of the most central concepts in thermodynamics and statistical mechanics. Due to its extremely wide applications on experimental measurements and theoretical studies, temperature is very important concept in both the thermal and sub-atomic physics. At least four types of temperatures can be found in literature of physics of high energy collisions, which includes the initial temperature, chemical freeze-out temperature, kinetic freeze-out temperature and effective temperature. These temperatures occur at different stages of the collision process. We have discussed some of these temperatures in our previous works [23, 24, 25, 26].

Three types of different freeze-out scenarios can be found in literature which includes single [27], double [28, 29] and multiple kinetic freeze-out scenarios [30, 31]. In single freeze-out scenario, one set of parameters should be used for both the spectra of strange

and non-strange particles [27], while one set of parameters for strange (or multi-strange) particles and other for non-strange (or non-multi-strange) particles should be used in double kinetic freeze-out scenario [28, 29]. Different sets of parameters for different particles with different masses should be used for multiple kinetic freeze-out scenario [30, 31]. It is needed to find out that which freeze-out scenario is correct.

In this article, we are focusing on the kinetic freeze-out temperature T_0 and transverse flow velocity β_T . We are interested in the onset energy of phase transition and the kinetic freeze-out scenario which can be obtained from the analysis of T_0 and β_T . We shall extract the two parameters from the transverse momentum (mass) spectra of different particles by using the blast-wave fit with Tsallis statistics.

The remainder of the paper includes the method and formalism, results and discussion, as well as summary and conclusions which are presented in sections 2, 3 and 4, respectively.

2 The method and formalism

We discuss the complex process of high energy collisions in the framework of the blast-wave fit with Tsallis statistics [27]. Various distributions can be used to describe the multiple emission sources and the complex structure of p_T spectra, which include but are not limited to the Erlang distribution [32], the standard distribution (Boltzmann, Fermi-Dirac and Bose-Einstein distributions) [33], the Tsallis distribution [34, 35, 36], the Tsallis+standard distribution [37, 38, 39, 40, 41, 42], the Schwinger mechanism [43, 44], the blast-wave fit with boltzmann statistics [45, 46, 47, 48] and so forth. These can be the choices in the soft excitation process. Although the probability density function can be of various forms, it is not enough to describe the p_T spectra, particularly the maximum p_T up to 100 GeV/c in collisions at LHC [49].

In fact, several p_T regions, including the first region with $p_T < 4-6$ GeV/c, the second region with $4-6$ GeV/c $< p_T < 17-20$ GeV/c and the third region with $p_T > 17-20$ GeV/c have been observed in ref. [50]. Different p_T regions are expected to correspond to different mechanisms. According to ref. [50], different whole features of fragmentation and hadronization of partons through the string dynamics can be reflected by different p_T regions. The effect and changes by the medium in the first p_T region take part in the main role, while

in second p_T region, it appears weakly. The third p_T region reflects the negligible influence of the medium on the nuclear transparency. Maximum number of strings are expected to have in the second p_T region from every point of view and it results in fusion and creation of strings and the partons collective behavior.

We would like to point out that we mention about different p_T regions corresponding to different mechanisms. This may be translated into having different fitting functions with different parameters when one fits the spectra in these regions. However, on the other hand, there are universality, similarity or common characteristic in high energy collisions [51, 52, 53, 54, 55, 56, 57, 58]. This means that one may also use the same function to fit the spectra in wide p_T range with the same fitting parameters. In fact, in ref. [59], the Tsallis-like distribution is able to fit the ATLAS and CMS spectra over 14 orders of magnitude with the same value of the parameters. Indeed, there are both the particular and common characteristics in high energy collisions.

Although various distributions may be used for describing the particle spectra, the Tsallis distribution and its alternative forms can fit the wider spectra. In particular, the Tsallis distribution can cover the two- or three-component standard distribution [60]. This means that, to fit the spectra as widely as possible, one may use the Tsallis distribution and its alternative forms. In addition, the blast-wave fit can be easily used to extract synchronously the kinetic freeze-out temperature T_0 and transverse flow velocity β_T . Thus, it is convenient for us to use the combination of the Tsallis distribution and the blast-wave fit to extract T_0 and β_T from enough wide spectra. This combination is in fact the the blast-wave fit with Tsallis statistics [27, 61].

According to [27], the probability density function of p_T at mid-rapidity in the blast-wave fit with Tsallis statistics can be given by

$$f_S(p_T) = C p_T m_T \int_{-\pi}^{\pi} d\phi \int_0^R r dr \left\{ 1 + \frac{q-1}{T_0} \times \left[m_T \cosh(\rho) - p_T \sinh(\rho) \cos(\phi) \right] \right\}^{-\frac{q}{q-1}}, \quad (1)$$

where C is the normalization constant, which results in the integral of Eq. (1) to be normalized to 1, $m_T = \sqrt{p_T^2 + m_0^2}$ and m_0 is the rest mass, ϕ and r denote the azimuthal angle and radial coordinate respectively, R is the maximum r , q is the entropy index, T_0 is the kinetic freeze out temperature, $\rho = \tanh^{-1}[\beta(r)]$ is the boost

angle, $\beta(r) = \beta_S(r/R)^{n_0}$ is a self-similar flow profile, β_S is the flow velocity on the surface and $n_0 = 1$ according to ref. [27]. Particularly $\beta_T = (2/R^2) \int_0^R r \beta(r) dr = 2\beta_S/(n_0 + 2) = 2\beta_S/3$.

It should be noted that the index $q/(q-1)$ [62] used in Eq. (1) is a replacement of $1/(q-1)$ used in refs. [27, 61] due to the fact that q is also required for the thermodynamic consistency [36, 62]. Because of q being close to 1, this replacement causes a very small difference in the values of q in the two cases. In addition, Eq. (1) is valid only at around mid-rapidity due to the fact that we have used $m_T \cosh y \approx m_T$ to simplify the equation from the integral of y . This simplification affects the normalization constant C , but there is no obvious influence on T_0 and β_T due to narrow mid-rapidity range being used. If the rapidity range is not around $y = 0$, we may transform it to around $y = 0$ to subtract the influence of longitudinal motion of emission source. As the normalization constant for the probability density function Eq. (1), C does not affect the free parameters.

In this paper, we use the blast-wave fit with Tsallis statistics to describe the soft excitation process. But in some cases the fit in high p_T region is not well, then we can use the two-component fit in which the second component describes the hard scattering process. The Hagedorn function [63, 64] or inverse power law [65, 66, 67] can be used for the second component, that is

$$f_H(p_T) = A p_T \left(1 + \frac{p_T}{p_0} \right)^{-n}, \quad (2)$$

where A is the normalization constant which results in the integral of Eq. (2) to be normalized to 1, and p_0 and n are the free parameters.

For the harder part of the spectra, we suggest to use the Hagedorn function given by Eq. (2) which is similar to the Tsallis-like function without the blast-wave corrections [36, 62]. In fact, there is a relation $n = q/(q-1)$ between the two functions. It is acceptable if we use the Tsallis-like function instead of the Hagedorn function in the case of the two temperatures (two entropy indexes) being distinguished for with and without the blast-wave corrections. The blast-wave corrections are not needed for the harder part of the spectra due to its earlier production than the softer part, when the blast-wave is not formed.

To describe the spectra in a wide p_T range, we have two methods to superpose Eqs. (1) and (2). That is

$$f_0(p_T) = k f_S(p_T) + (1 - k) f_H(p_T) \quad (3)$$

and

$$f_0(p_T) = A_1\theta(p_1 - p_T)f_S(p_T) + A_2\theta(p_T - p_1)f_H(p_T), \quad (4)$$

where k ($1 - k$) denotes the contribution fraction of the soft excitation (hard scattering) process in the first method. Naturally, the integral of Eq. (3) is normalized to 1. Meanwhile, in the second method [63], A_1 and A_2 are the normalization constants which result in the two components to be equal to each other at $p_T = p_1$. The function $\theta(x) = 0$ if $x < 0$ and $\theta(x) = 1$ if $x \geq 0$. The integral of Eq. (4) is normalized to 1, too. The contribution fraction k ($1 - k$) of the soft excitation (hard scattering) process in the second method is the integral of the first (second) component in Eq. (4).

To use Eq. (4) and to decide the value of p_1 , we may fit the low- and high- p_T regions by the first and second components respectively [25]. It is general that the first component cannot fit the high- p_T region and the second component cannot fit the low- p_T region. There is a cross connection between the two components. The value of p_T at the cross connection is naturally regarded as the value of p_1 . Because of the cross connection is restricted by the two components, p_1 is not a free parameter. Generally, the curve at $p_T = p_1$ is possibly not too smooth.

If the spectra are not in a very wide p_T range, the second component in Eqs. (3) and (4) are not necessary in the fitting procedure. Thus, we can use only the first component in Eqs. (3) and (4), that is Eq. (1), to fit the spectra. Although Eqs. (2)–(4) are not used in the fitting procedure in this work, we present them to show a whole treatment in methodology. In the case of analyzing the spectra in wide p_T range, we may use together Eqs. (1) and (2) due to Eq. (3) or (4).

In some cases, the spectra are in the form of m_T , but not p_T . Then, we need to convert the p_T distribution $f_S(p_T)$ to the m_T distribution $f_{S'}(m_T)$ by $f_{S'}(m_T)|dm_T| = f_S(p_T)|dp_T|$ through $p_T|dp_T| = m_T|dm_T|$ due to the invariant cross-section. In fact, Eq. (1) used in ref. [27] appearing in the form of $f_{S'}(m_T)$. We convert it to the form of $f_S(p_T)$ expediently. To extract T_0 and β_T , we do not need the spectra in a wide p_T range due to small fraction in high p_T region.

3 Results and discussion

Figures 1(a)–1(d) and the continued part Figures 1(e)–1(h) demonstrate the p_T or m_T –

m_0 spectra, $(1/2\pi p_T)d^2N/dp_T dy$, $d^2N/dp_T dy$, $(1/2\pi m_T)d^2N/dm_T dy$, or $(1/m_T^2)d^2N/dm_T dy$, of the non-multi-strange (i.e. other identified) particles (π^+ , K^+ , p , K_S^0 and Λ) and multi-strange particles [ϕ , Ξ^+ , Ξ^- , Ξ] and $\bar{\Omega}^+$ ($\Omega^- + \Omega^+$, Ω), produced at mid-rapidity (mid- y) or mid-pseudorapidity (mid- η) in central Au-Au, Pb-Pb, Ar-KCl and Ni-Ni collisions at different $\sqrt{s_{NN}}$, the center-of-mass energy per nucleon pair, where N denotes the number of particles. The particle types and collision energies are marked in the panels. The symbols in panels (a)–(c) represent the experimental data measured by the E866 [68], E895 [69, 70], E802 [71, 72], STAR [73, 74, 75], PHENIX [76, 77] and ALICE collaborations [78]. In panel (d) the symbols represent the experimental data measured by the HADES [79, 80], STAR [81, 82, 83] and CMS Collaborations [84]. The symbols in panels (e), (f), (g) and (h) represent the experimental data quoted from refs. [81, 85, 86], [81, 87, 88, 89], [81, 88, 89] and [76, 77, 84, 85], respectively. The curves are our fitted results by using Eq. (1). The values of the free parameters (T_0 , β_T and q), the normalization constant (N_0), χ^2 , and the number of degree of freedom (ndof) are given in Table 1 and its continued part with together the concrete collisions, energies, centrality, (pseudo)rapidity, particles, spectra and scaled factors in the figure. Due to the resonance production, the spectra in very low- p_T region are not taken care carefully in the fit process, while the fit itself is not too good. One can see that the blast-wave fit with Tsallis statistics fits approximately the experimental data over a wide energy range.

It should be noted that the normalization constant N_0 is used to compare the fit function $f_S(p_T)$ (or $f_{S'}(m_T)$) and the experimental spectra, and the normalization constant C is used to let the integral of Eq. (1) be 1. The two normalization constants are different, though C can be absorbed in N_0 . We have used both the C and N_0 to give a clear description. In the comparisons, we have $(1/2\pi p_T)N_0 f_S(p_T)/dy = (1/2\pi p_T)d^2N/dp_T dy$, $N_0 f_S(p_T)/dy = d^2N/dp_T dy$, $(1/2\pi m_T)N_0 f_{S'}(m_T)/dy = (1/2\pi m_T)d^2N/dm_T dy$, or $(1/m_T^2)N_0 f_{S'}(m_T)/dy = (1/m_T^2)d^2N/dm_T dy$, due to different forms of the spectra. In particular, the value of N_0 for K_S^0 production in Ar-KCl collisions at 2.25 GeV is very small due to less participant nucleons at lower collision energy performed in ref. [79].

Table 1. Values of T_0 , β_T , q , N_0 , χ^2 , and ndof corresponding to the curves in Fig. 1, where the centrality classes, (pseudo)rapidity ranges, types of spectra and the scaled factors are listed. The scaled factors are just used for the display purpose only.

Figure	Energy	Centrality	y (η)	Particle	Spectrum	Scaled	T_0 (GeV)	β_T (c)	q	N_0	χ^2	ndof	
Fig. 1(a) Au-Au	2.7 GeV	0-5%	$ y < 0.05$	π^+	$(1/2\pi m_T)d^2N/dm_T dy$	1/4	0.024 ± 0.005	0.339 ± 0.009	1.130 ± 0.020	0.80 ± 0.05	3	22	
	3.32 GeV	0-5%	$ y < 0.05$		$(1/2\pi m_T)d^2N/dm_T dy$	1/3	0.031 ± 0.004	0.344 ± 0.008	1.150 ± 0.030	2.07 ± 0.20	2	27	
	3.8 GeV	0-5%	$ y < 0.05$		$(1/2\pi m_T)d^2N/dm_T dy$	1/2	0.038 ± 0.006	0.358 ± 0.015	1.120 ± 0.010	3.08 ± 0.20	33	22	
	4.3 GeV	0-5%	$ y < 0.05$		$(1/2\pi m_T)d^2N/dm_T dy$	-	0.050 ± 0.004	0.376 ± 0.016	1.060 ± 0.010	3.28 ± 0.33	50	19	
	5.03 GeV	0-5%	$0 < y < 0.4$		$(1/2\pi m_T)d^2N/dm_T dy$	2	0.060 ± 0.005	0.390 ± 0.010	1.086 ± 0.005	7.10 ± 1.00	96	34	
	7.7 GeV	0-5%	$ y < 0.1$		$(1/2\pi p_T)d^2N/dp_T dy$	-	0.068 ± 0.004	0.429 ± 0.008	1.058 ± 0.005	15.33 ± 2.00	113	26	
	11.5 GeV	0-5%	$ y < 0.1$		$(1/2\pi p_T)d^2N/dp_T dy$	2	0.067 ± 0.005	0.430 ± 0.008	1.069 ± 0.006	19.43 ± 2.80	119	26	
	14.5 GeV	0-5%	$ y < 0.1$		$(1/2\pi p_T)d^2N/dp_T dy$	4	0.068 ± 0.004	0.428 ± 0.006	1.080 ± 0.007	21.93 ± 2.20	153	28	
	19.6 GeV	0-5%	$ y < 0.1$		$(1/2\pi p_T)d^2N/dp_T dy$	8	0.068 ± 0.005	0.429 ± 0.009	1.058 ± 0.028	25.20 ± 4.00	178	26	
	27 GeV	0-5%	$ y < 0.1$		$(1/2\pi p_T)d^2N/dp_T dy$	16	0.069 ± 0.004	0.430 ± 0.009	1.080 ± 0.006	26.43 ± 2.25	49	26	
	39 GeV	0-5%	$ y < 0.1$		$(1/2\pi p_T)d^2N/dp_T dy$	32	0.069 ± 0.005	0.430 ± 0.008	1.080 ± 0.007	28.43 ± 3.50	93	26	
	62.4 GeV	0-5%	$ y < 0.1$		$(1/2\pi p_T)d^2N/dp_T dy$	64	0.076 ± 0.006	0.447 ± 0.007	1.040 ± 0.008	32.53 ± 2.50	63	10	
	130 GeV	0-5%	$ \eta < 0.35$		$(1/2\pi p_T)d^2N/dp_T dy$	120	0.082 ± 0.006	0.478 ± 0.008	1.031 ± 0.006	34.43 ± 2.70	3	14	
	200 GeV	0-5%	$ \eta < 0.35$		$(1/2\pi p_T)d^2N/dp_T dy$	240	0.089 ± 0.005	0.489 ± 0.009	1.024 ± 0.008	95.80 ± 10.00	94	28	
	Pb-Pb	2.76 TeV	0-5%	$ y < 0.5$		$(1/2\pi p_T)d^2N/dp_T dy$	-	0.094 ± 0.006	0.500 ± 0.011	1.040 ± 0.007	122.00 ± 10.00	90	41
Fig. 1(b) Au-Au	2.7 GeV	0-5%	$ y < 0.23$	K^+	$(1/2\pi m_T)d^2N/dm_T dy$	-	0.027 ± 0.006	0.300 ± 0.015	1.001 ± 0.008	0.014 ± 0.005	1	10	
	3.32 GeV	0-5%	$ y < 0.29$		$(1/2\pi m_T)d^2N/dm_T dy$	-	0.033 ± 0.006	0.317 ± 0.016	1.014 ± 0.005	0.080 ± 0.004	1	12	
	3.8 GeV	0-5%	$ y < 0.34$		$(1/2\pi m_T)d^2N/dm_T dy$	1.2	0.040 ± 0.007	0.331 ± 0.012	1.001 ± 0.008	0.20 ± 0.04	5	11	
	4.3 GeV	0-5%	$ y < 0.37$		$(1/2\pi m_T)d^2N/dm_T dy$	2	0.048 ± 0.006	0.347 ± 0.012	1.001 ± 0.008	0.30 ± 0.05	4	9	
	5.03 GeV	0-5%	$ y < 0.1$		$(1/2\pi m_T)d^2N/dm_T dy$	3	0.059 ± 0.005	0.362 ± 0.010	1.001 ± 0.007	0.60 ± 0.03	11	11	
	7.7 GeV	0-5%	$ y < 0.1$		$(1/2\pi p_T)d^2N/dp_T dy$	-	0.072 ± 0.004	0.397 ± 0.007	1.055 ± 0.006	3.28 ± 0.40	9	23	
	11.5 GeV	0-5%	$ y < 0.1$		$(1/2\pi p_T)d^2N/dp_T dy$	2	0.073 ± 0.005	0.398 ± 0.004	1.055 ± 0.007	4.00 ± 0.50	32	25	
	14.5 GeV	0-5%	$ y < 0.1$		$(1/2\pi p_T)d^2N/dp_T dy$	4	0.073 ± 0.005	0.398 ± 0.004	1.061 ± 0.007	4.33 ± 0.50	67	26	
	19.6 GeV	0-5%	$ y < 0.1$		$(1/2\pi p_T)d^2N/dp_T dy$	8	0.073 ± 0.006	0.397 ± 0.008	1.065 ± 0.008	4.73 ± 0.70	11	26	
	27 GeV	0-5%	$ y < 0.1$		$(1/2\pi p_T)d^2N/dp_T dy$	16	0.073 ± 0.006	0.398 ± 0.007	1.066 ± 0.009	4.80 ± 0.55	19	26	
	39 GeV	0-5%	$ y < 0.1$		$(1/2\pi p_T)d^2N/dp_T dy$	32	0.073 ± 0.004	0.398 ± 0.007	1.056 ± 0.007	5.00 ± 0.60	12	26	
	62.4 GeV	0-5%	$ y < 0.1$		$(1/2\pi p_T)d^2N/dp_T dy$	64	0.079 ± 0.005	0.415 ± 0.008	1.064 ± 0.385	5.93 ± 0.50	1	10	
	130 GeV	0-5%	$ \eta < 0.35$		$(1/2\pi p_T)d^2N/dp_T dy$	120	0.084 ± 0.005	0.423 ± 0.011	1.035 ± 0.010	6.33 ± 0.70	12	13	
	200 GeV	0-5%	$ \eta < 0.35$		$(1/2\pi p_T)d^2N/dp_T dy$	340	0.090 ± 0.005	0.440 ± 0.009	1.052 ± 0.100	6.60 ± 0.60	1	16	
	Pb-Pb	2.76 TeV	0-5%	$ y < 0.5$		$(1/2\pi p_T)d^2N/dp_T dy$	-	0.096 ± 0.005	0.460 ± 0.009	1.090 ± 0.100	15.60 ± 0.60	23	36
Fig. 1(c) Au-Au	2.7 GeV	0-5%	$ y < 0.05$	p	$(1/2\pi m_T)d^2N/dm_T dy$	-	0.030 ± 0.005	0.280 ± 0.008	1.010 ± 0.006	2.53 ± 0.16	72	39	
	3.32 GeV	0-5%	$ y < 0.05$		$(1/2\pi m_T)d^2N/dm_T dy$	2.5	0.035 ± 0.004	0.291 ± 0.007	1.010 ± 0.010	2.34 ± 0.16	57	39	
	3.8 GeV	0-5%	$ y < 0.05$		$(1/2\pi m_T)d^2N/dm_T dy$	6	0.041 ± 0.008	0.307 ± 0.016	1.010 ± 0.006	2.27 ± 0.16	151	39	
	4.3 GeV	0-5%	$ y < 0.05$		$(1/2\pi m_T)d^2N/dm_T dy$	16	0.062 ± 0.006	0.317 ± 0.013	1.005 ± 0.006	2.16 ± 0.10	73	36	
	5.03 GeV	0-5%	$0 < y < 0.2$		$(1/2\pi m_T)d^2N/dm_T dy$	30	0.057 ± 0.007	0.331 ± 0.011	1.001 ± 0.007	2.43 ± 0.20	49	29	
	7.7 GeV	0-5%	$ y < 0.1$		$(1/2\pi p_T)d^2N/dp_T dy$	50	0.075 ± 0.007	0.407 ± 0.010	1.030 ± 0.004	8.59 ± 0.60	12	29	
	11.5 GeV	0-5%	$ y < 0.1$		$(1/2\pi p_T)d^2N/dp_T dy$	200	0.075 ± 0.005	0.407 ± 0.007	1.027 ± 0.010	7.13 ± 0.40	8	28	
	14.5 GeV	0-5%	$ y < 0.1$		$(1/2\pi p_T)d^2N/dp_T dy$	600	0.075 ± 0.005	0.408 ± 0.008	1.034 ± 0.006	6.18 ± 0.27	10	25	
	19.6 GeV	0-5%	$ y < 0.1$		$(1/2\pi p_T)d^2N/dp_T dy$	1300	0.076 ± 0.004	0.407 ± 0.007	1.033 ± 0.010	5.61 ± 0.50	21	29	
	27 GeV	0-5%	$ y < 0.1$		$(1/2\pi p_T)d^2N/dp_T dy$	2900	0.076 ± 0.006	0.407 ± 0.008	1.041 ± 0.010	4.83 ± 0.60	11	23	
	39 GeV	0-5%	$ y < 0.1$		$(1/2\pi p_T)d^2N/dp_T dy$	7000	0.076 ± 0.006	0.407 ± 0.008	1.048 ± 0.010	4.13 ± 0.60	16	22	
	62.4 GeV	0-5%	$ y < 0.1$		$(1/2\pi p_T)d^2N/dp_T dy$	14000	0.081 ± 0.004	0.411 ± 0.008	1.080 ± 0.012	4.68 ± 0.27	3	15	
	130 GeV	0-5%	$ \eta < 0.35$		$(1/2\pi p_T)d^2N/dp_T dy$	28000	0.086 ± 0.006	0.418 ± 0.009	1.040 ± 0.007	4.33 ± 0.30	12	17	
	200 GeV	0-5%	$ \eta < 0.35$		$(1/2\pi p_T)d^2N/dp_T dy$	1/20	0.091 ± 0.004	0.428 ± 0.007	1.050 ± 0.008	4.33 ± 0.33	10	22	
	Pb-Pb	2.76 TeV	0-5%	$ y < 0.5$		$(1/2\pi p_T)d^2N/dp_T dy$	500	0.098 ± 0.004	0.441 ± 0.007	1.025 ± 0.008	5.02 ± 0.33	4	37
Fig. 1(d) Ar-KCl Au-Au	2.25 GeV	0-35%	$ y < 0.05$	K_S^0	$(1/m_T^2)d^2N/dy dm_T$	10^7	0.019 ± 0.007	0.232 ± 0.012	1.010 ± 0.007	0.0000090 ± 0.0000010	33	13	
	2.4 GeV	0-40%	$ y < 0.05$		$(1/m_T^2)d^2N/dy dm_T$	10^6	0.023 ± 0.006	0.242 ± 0.010	1.001 ± 0.020	0.0060 ± 0.0001	41	16	
	7.7 GeV	0-5%	$ y < 0.5$		$(1/2\pi p_T)d^2N/dp_T dy$	-	0.103 ± 0.006	0.390 ± 0.015	1.010 ± 0.008	1.97 ± 0.20	1	12	
	11.5 GeV	0-5%	$ y < 0.5$		$(1/2\pi p_T)d^2N/dp_T dy$	2	0.104 ± 0.005	0.393 ± 0.012	1.015 ± 0.008	2.37 ± 0.10	12	14	
	19.6 GeV	0-5%	$ y < 0.5$		$(1/2\pi p_T)d^2N/dp_T dy$	4	0.104 ± 0.006	0.393 ± 0.010	1.020 ± 0.008	3.17 ± 0.10	6	15	
	27 GeV	0-5%	$ y < 0.5$		$(1/2\pi p_T)d^2N/dp_T dy$	8	0.104 ± 0.007	0.392 ± 0.014	1.025 ± 0.009	3.77 ± 0.10	8	16	
	39 GeV	0-5%	$ y < 0.5$		$(1/2\pi p_T)d^2N/dp_T dy$	16	0.104 ± 0.006	0.392 ± 0.014	1.030 ± 0.007	3.90 ± 0.50	6	16	
	62.4 GeV	0-5%	$ y < 0.5$		$(1/2\pi m_T)d^2N/dm_T dy$	132	0.114 ± 0.007	0.401 ± 0.012	1.030 ± 0.009	5.30 ± 0.40	2	14	
	130 GeV	0-6%	$ y < 0.5$		$(1/2\pi m_T)d^2N/dm_T dy$	160	0.120 ± 0.008	0.412 ± 0.013	1.001 ± 0.009	5.30 ± 0.40	26	9	
	Pb-Pb	2.76 TeV	0-5%	$ y < 0.5$		$(1/2\pi p_T)d^2N/dp_T dy$	900	0.133 ± 0.005	0.432 ± 0.014	1.050 ± 0.011	0.98 ± 0.40	10	32

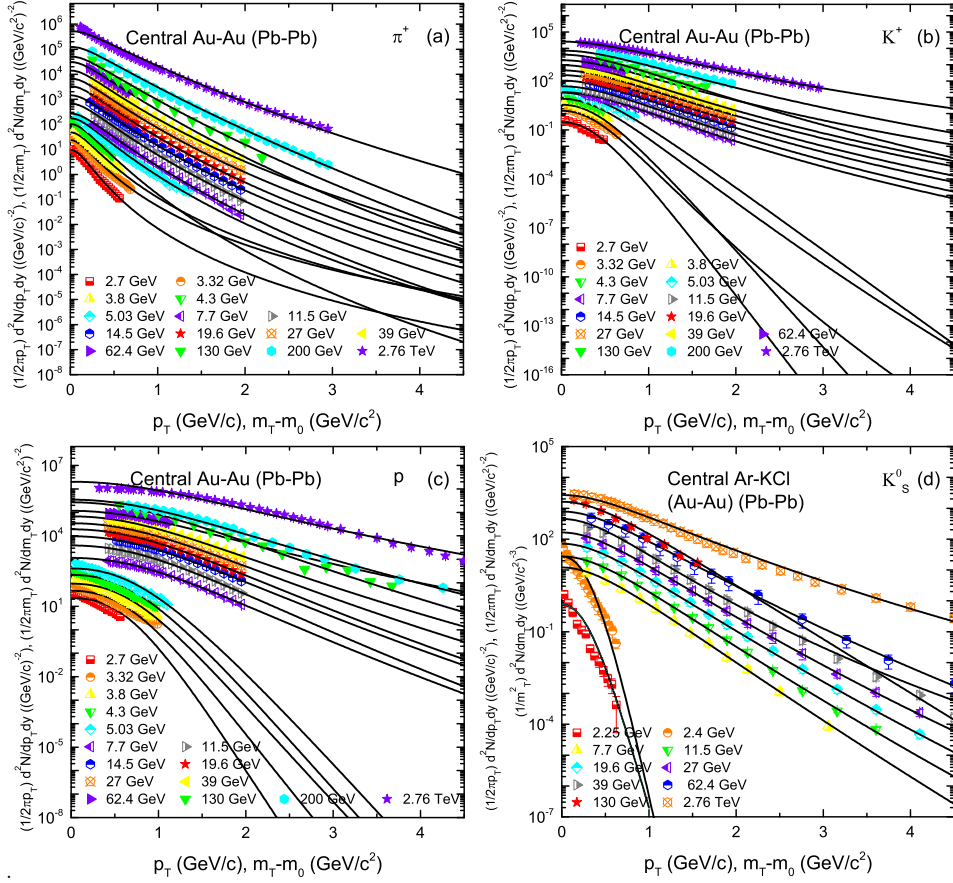


Fig. 1. The p_T or $m_T - m_0$ spectra, $(1/2\pi p_T)d^2N/dp_T dy$, $(1/2\pi m_T)d^2N/dm_T dy$, $d^2N/dp_T dy$, or $(1/m_T^2)d^2N/dm_T dy$, of other identified particles (π^+ , K^+ , p and K_S^0), produced at mid- y in central Au-Au, Pb-Pb and Ar-KCl collisions at different $\sqrt{s_{NN}}$. The particle types and collision energies are marked in the panels. The symbols in panels (a)–(c) represent the experimental data measured by the E866 [68], E895 [69, 70], E802 [71, 72], STAR [73, 74, 75], PHENIX [76, 77] and ALICE collaborations [78]. In panel (d) the symbols represent the experimental data measured by the HADES [79, 80], STAR [81, 82, 83] and CMS Collaborations [84]. The curves are our fitted results by using Eq. (1). More information in detail can be found in Table 1.

In addition, although R can be regarded as the transverse radius of the participant region, it has no absolute meaning due to the fact that it appears in terms of r/R . Although the fit result is not related to R , R cannot be absorbed in C or N_0 due to a concrete R being needed to perform the calculation process. As the simple normalization constant in probability density function and the irrelevant upper limit in integral process, the values of C and R are not listed in Table 1 to avoid trivial presentation.

Before continuing this work, we would like to point out that Fig. 1 is only a part collection of transverse spectra. In fact, more experimental data were published in the community. For example, the NA49 experiment was performed for carbon-carbon (C-C), silicon-

silicon (Si-Si) and Pb-Pb collisions in which the extensive experimental studies of the possible phase transition were carried in the range of $\sqrt{s_{NN}} = 6.3\text{--}17.3$ GeV [90, 91, 92, 93]. The NA61/SHINE experiment was performed at similar energies for gathering rich data on nuclear collisions in a two-dimensional scan, i.e. varying collision energy and nuclear size [92, 93, 94, 95]. Indeed, these experiments have provided more abundant data.

To study the dependence of kinetic freeze-out temperature T_0 and transverse flow velocity β_T on collision energy $\sqrt{s_{NN}}$, the excitation functions of T_0 and β_T for central Au-Au collisions are shown in Figs. 2(a) and 2(b) respectively. The results for π^+ , K^+ , p , K_S^0 , ϕ , Λ , Ξ^+ (Ξ^-) and Ω^+ ($\Omega^- + \Omega^+$, Ω) are represented by different symbols marked in the panels. One can

Table 1. Continued. Values of T_0 , β_T , q , N_0 , χ^2 , and ndof corresponding to the curves in Fig. 1 continued part, where the centrality classes, (pseudo)rapidity ranges, types of spectra and the scaled factors are listed. The scaled factors are just used for the display purpose only.

Figure	Energy	Centrality	y (η)	Particle	Spectrum	Scaled	T_0 (GeV)	β_T (c)	q	N_0	χ^2	ndof		
Fig. 1(e)	7.7 GeV	0-5%	$ y < 0.5$	ϕ	$(1/2\pi p_T)d^2N/dp_T dy$	–	0.108 ± 0.007	0.350 ± 0.014	1.030 ± 0.010	0.20 ± 0.03	1	7		
	Au-Au	11.5 GeV	0-5%		$ y < 0.5$	$(1/2\pi p_T)d^2N/dp_T dy$	2	0.108 ± 0.006	0.351 ± 0.013	1.021 ± 0.007	0.27 ± 0.01	2	10	
		19.6 GeV	0-5%		$ y < 0.5$	$(1/2\pi p_T)d^2N/dp_T dy$	4	0.109 ± 0.007	0.350 ± 0.014	1.022 ± 0.007	0.41 ± 0.01	1	11	
		27 GeV	0-5%		$ y < 0.5$	$(1/2\pi p_T)d^2N/dp_T dy$	8	0.109 ± 0.006	0.351 ± 0.015	1.026 ± 0.011	0.50 ± 0.03	2	12	
		39 GeV	0-5%		$ y < 0.5$	$(1/2\pi p_T)d^2N/dp_T dy$	16	0.108 ± 0.008	0.351 ± 0.016	1.030 ± 0.009	0.54 ± 0.01	4	12	
		130 GeV	0-11%		$ y < 0.5$	$(1/2\pi m_T)d^2N/dm_T dy$	50	0.124 ± 0.005	0.370 ± 0.013	1.050 ± 0.009	0.27 ± 0.04	14	9	
		200 GeV	0-10%		$ y < 0.5$	$(1/2\pi p_T)d^2N/dp_T dy$	100	0.133 ± 0.006	0.380 ± 0.014	1.030 ± 0.008	1.24 ± 0.40	2	14	
Pb-Pb	2.76 TeV	0-5%	$ y < 0.5$		$d^2N/dp_T dy$	10	0.140 ± 0.005	0.391 ± 0.012	1.035 ± 0.010	48.00 ± 0.40	4	8		
Fig. 1(f) Ni-Ni	2.32 GeV	0-5%	$-1 < y < 0$	Λ	$(1/m_T^2)d^2N/dy dm_T$	10^8	0.030 ± 0.005	0.199 ± 0.015	1.001 ± 0.007	0.00076 ± 0.00003	17	9		
	Au-Au	7.7 GeV	0-5%		$ y < 0.5$	$(1/2\pi p_T)d^2N/dp_T dy$	–	0.114 ± 0.006	0.312 ± 0.012	1.015 ± 0.008	2.20 ± 0.20	5	13	
		11.5 GeV	0-5%		$ y < 0.5$	$(1/2\pi p_T)d^2N/dp_T dy$	2	0.115 ± 0.006	0.313 ± 0.012	1.018 ± 0.008	2.10 ± 0.10	5	14	
		19.6 GeV	0-5%		$ y < 0.5$	$(1/2\pi p_T)d^2N/dp_T dy$	4	0.115 ± 0.005	0.313 ± 0.013	1.022 ± 0.007	1.95 ± 0.10	11	15	
		27 GeV	0-5%		$ y < 0.5$	$(1/2\pi p_T)d^2N/dp_T dy$	8	0.114 ± 0.006	0.312 ± 0.013	1.027 ± 0.009	1.95 ± 0.10	9	15	
		39 GeV	0-5%		$ y < 0.5$	$(1/2\pi p_T)d^2N/dp_T dy$	16	0.115 ± 0.007	0.313 ± 0.012	1.035 ± 0.008	1.78 ± 0.50	7	14	
		62.4 GeV	0-5%		$ y < 0.05$	$(1/2\pi p_T)d^2N/dp_T dy$	32	0.125 ± 0.005	0.325 ± 0.012	1.029 ± 0.009	1.78 ± 0.40	9	12	
		130 GeV	0-5%		$ y < 0.05$	$(1/2\pi p_T)d^2N/dp_T dy$	64	0.132 ± 0.006	0.337 ± 0.014	1.040 ± 0.020	2.17 ± 0.40	9	10	
		200 GeV	0-5%		$ y < 0.05$	$(1/2\pi p_T)d^2N/dp_T dy$	120	0.140 ± 0.006	0.348 ± 0.011	1.028 ± 0.030	2.67 ± 0.40	22	17	
	Pb-Pb	2.76 TeV	0-5%		$ y < 0.05$		$d^2N/dp_T dy$	70	0.149 ± 0.007	0.359 ± 0.012	1.045 ± 0.013	19.78 ± 3.00	27	19
Fig. 1(g)	7.7 GeV	0-5%	$ y < 0.5$	Ξ^+	$(1/2\pi p_T)d^2N/dp_T dy$	–	0.119 ± 0.006	0.289 ± 0.011	1.022 ± 0.011	0.010 ± 0.003	2	6		
	Au-Au	11.5 GeV	0-5%		$ y < 0.5$	$(1/2\pi p_T)d^2N/dp_T dy$	2	0.120 ± 0.005	0.290 ± 0.012	1.022 ± 0.008	0.27 ± 0.01	3	7	
		19.6 GeV	0-5%		$ y < 0.5$	$(1/2\pi p_T)d^2N/dp_T dy$	4	0.120 ± 0.005	0.290 ± 0.012	1.025 ± 0.007	0.080 ± 0.001	4	7	
		27 GeV	0-5%		$ y < 0.5$	$(1/2\pi p_T)d^2N/dp_T dy$	8	0.120 ± 0.006	0.290 ± 0.014	1.026 ± 0.012	0.11 ± 0.03	5	8	
		39 GeV	0-5%		$ y < 0.5$	$(1/2\pi p_T)d^2N/dp_T dy$	16	0.120 ± 0.006	0.290 ± 0.013	1.026 ± 0.009	0.20 ± 0.008	8	8	
		62.4 GeV	0-5%	$ y < 0.05$	Ξ^+	$(1/2\pi p_T)d^2N/dp_T dy$	32	0.127 ± 0.007	0.304 ± 0.013	1.027 ± 0.009	0.20 ± 0.04	31	11	
		130 GeV	0-5%	$ y < 0.05$		$(1/2\pi p_T)d^2N/dp_T dy$	64	0.135 ± 0.005	0.315 ± 0.014	1.037 ± 0.008	0.27 ± 0.04	11	10	
		200 GeV	0-5%	$ y < 0.05$		$(1/2\pi p_T)d^2N/dp_T dy$	150	0.142 ± 0.005	0.325 ± 0.012	1.040 ± 0.008	0.27 ± 0.05	28	15	
	Pb-Pb	2.76 TeV	0-5%	$ y < 0.05$			$d^2N/dp_T dy$	40	0.150 ± 0.006	0.334 ± 0.015	1.053 ± 0.012	5.27 ± 0.80	5	12
	Fig. 1(h)	7.7 GeV	0-5%	$ y < 0.5$		Ω^+	$(1/2\pi p_T)d^2N/dp_T dy$	–	0.125 ± 0.005	0.243 ± 0.012	1.012 ± 0.011	0.0013 ± 0.0003	1	5
Au-Au		11.5 GeV	0-5%	$ y < 0.5$	$(1/2\pi p_T)d^2N/dp_T dy$		2	0.125 ± 0.005	0.243 ± 0.012	1.012 ± 0.009	0.0060 ± 0.0005	6	6	
		19.6 GeV	0-5%	$ y < 0.5$	$(1/2\pi p_T)d^2N/dp_T dy$		4	0.125 ± 0.005	0.244 ± 0.013	1.030 ± 0.007	0.012 ± 0.002	5	6	
		27 GeV	0-5%	$ y < 0.5$	$(1/2\pi p_T)d^2N/dp_T dy$		8	0.126 ± 0.006	0.244 ± 0.014	1.040 ± 0.014	0.015 ± 0.003	4	6	
		39 GeV	0-5%	$ y < 0.5$	$(1/2\pi p_T)d^2N/dp_T dy$		16	0.126 ± 0.007	0.243 ± 0.015	1.035 ± 0.008	0.020 ± 0.006	14	10	
		62.4 GeV	0-5%	$ y < 0.05$	$(1/2\pi p_T)d^2N/dp_T dy$		32	0.134 ± 0.006	0.253 ± 0.010	1.025 ± 0.008	0.26 ± 0.04	1	5	
		130 GeV	0-5%	$ y < 0.05$	$\Omega^- + \Omega^+$		$(1/2\pi p_T)d^2N/dp_T dy$	64	0.142 ± 0.006	0.265 ± 0.015	1.065 ± 0.008	0.090 ± 0.004	2	4
		200 GeV	0-5%	$ y < 0.05$			$(1/2\pi p_T)d^2N/dp_T dy$	200	0.149 ± 0.007	0.271 ± 0.014	1.045 ± 0.008	2.00 ± 0.20	14	5
Pb-Pb		2.76 TeV	0-5%	$ y < 0.05$				$d^2N/dp_T dy$	40	0.155 ± 0.006	0.278 ± 0.014	1.065 ± 0.013	0.75 ± 0.06	2

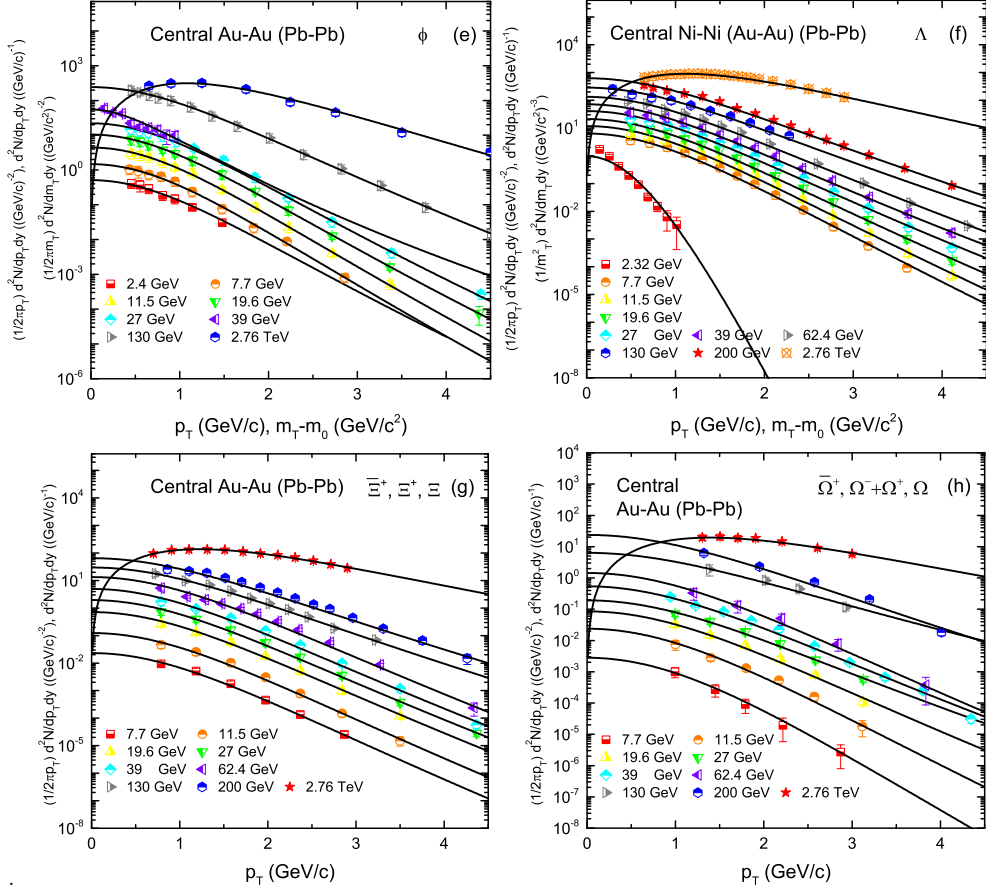


Fig.1. Continued. The same as for Figure 1, but showing the p_T or $m_T - m_0$ spectra of other identified particles (Λ) and multi-strange particles [ϕ , Ξ^+ (Ξ^+ , Ξ) and $\bar{\Omega}^+$ ($\Omega^- + \Omega^+$, Ω)] produced at mid- y in central Au-Au, Pb-Pb and Ni-Ni collisions at different $\sqrt{s_{NN}}$. The symbols in panels (e), (f), (g) and (h) represent the experimental data quoted from refs. [81, 85, 86], [81, 87, 88, 89], [81, 88, 89] and [76, 77, 84, 85], respectively. More information in detail can be found in Table 1 continued part.

see that T_0 in Fig. 2(a) and β_T in Fig. 2(b) increase quickly at lower energies from 2.7 to 7.7 GeV due to the fact that the system got higher excitation degree and stronger squeeze and expansion degree. They remain constant from 7.7 to 39 GeV and then increase up to higher energies. The variation of T_0 and β_T at different collision energies is displayed in Fig. 2(c). A larger T_0 can be clearly seen at larger β_T due to higher collision energy, which shows positive correlation between T_0 and β_T .

We notice that there is a saturation in the excitation functions of T_0 and β_T in the BES energy range at the RHIC, which means that the interaction mechanism or evolution process in $\sqrt{s_{NN}} = 7.7\text{--}39$ GeV is different from that in $\sqrt{s_{NN}} < 7.7$ GeV and in $\sqrt{s_{NN}} > 39$ GeV. In our opinion, the system is baryon-dominated in $\sqrt{s_{NN}} < 7.7$ GeV, in which there is no phase tran-

sition from hadron matter to QGP due to small energy deposition. The system is meson-dominated in $\sqrt{s_{NN}} > 39$ GeV, in which the phase transition had happened in whole volume due to large energy deposition. The system starts its phase transition in part volume at $\sqrt{s_{NN}} = 7.7$ GeV and undergoes from baryon-dominated to meson-dominated due to phase transition in larger and larger volume in $\sqrt{s_{NN}} = 7.7\text{--}39$ GeV. The onset energy of part phase transition is 7.7 GeV and that of whole phase transition is 39 GeV. The critical energy range is from 7.7 GeV to 39 GeV.

It is known that the chemical freeze-out temperature T_{ch} and baryon chemical potential μ_B from the thermal and statistical model [96, 97], can be parameterized as

$$T_{ch} = \frac{T_{lim}}{1 + \exp[2.60 - \ln(\sqrt{s_{NN}})/0.45]} \quad (5)$$

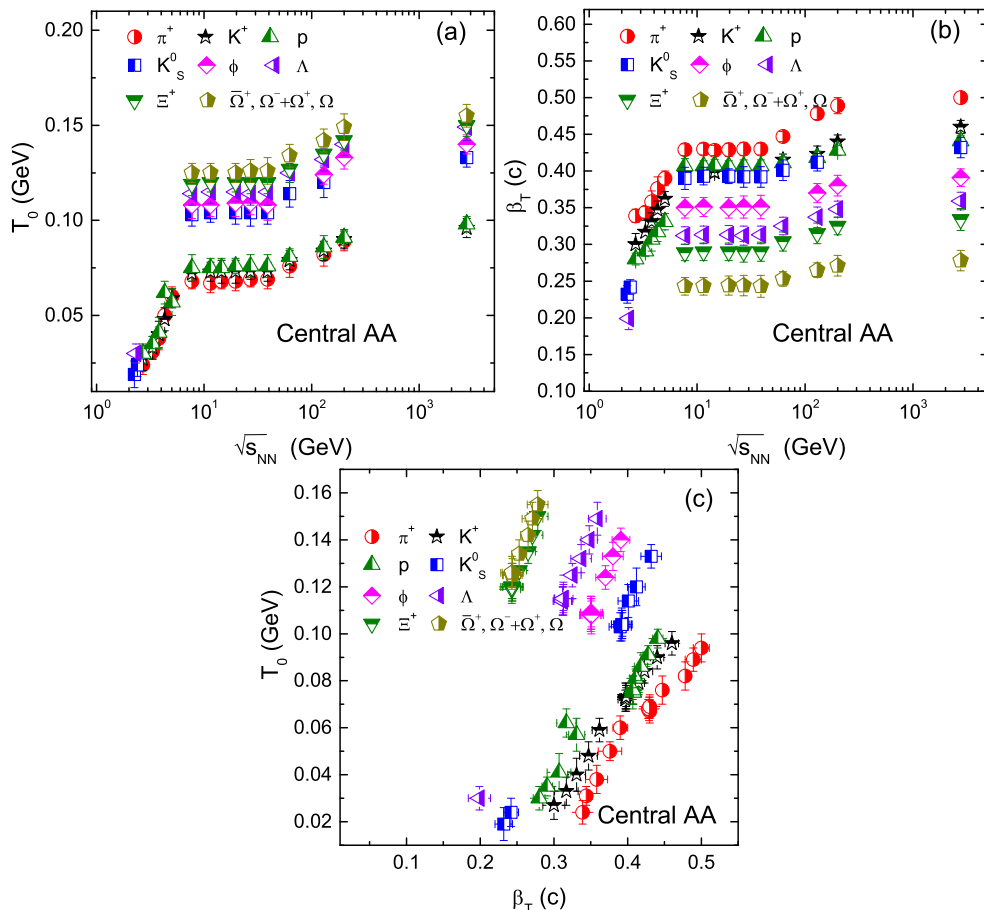


Fig. 2. Dependence of (a) T_0 on $\sqrt{s_{NN}}$, (b) β_T on $\sqrt{s_{NN}}$ and (c) T_0 on β_T for different $\sqrt{s_{NN}}$ in central AA collisions. The symbols marked in the panels represent the parameter values listed in Table 1 and its continued part.

and

$$\mu_B = \frac{a}{1 + 0.288\sqrt{s_{NN}}}, \quad (6)$$

where $T_{lim} = 0.1584$ GeV, $a = 1.3075$ GeV, and $\sqrt{s_{NN}}$ is in the units of GeV [98]. We have the critical range of $T_{ch} = 0.138$ – 0.158 GeV and $\mu_B = 0.406$ – 0.107 GeV while $\sqrt{s_{NN}} = 7.7$ – 39 GeV. These values show the ranges of T_{ch} and μ_B in the critical energy range.

We noticed that it is indeed possible to observe that while going from low to high temperature, a hadron gas becomes more and more meson dominated. As mentioned in ref. [99], with the help of the thermal model calculations, it is possible to plot the normalized entropy density for mesons and baryons, and then one may observe that the dominance changes at a cross-over temperature of $T_{ch} \approx 0.140$ GeV corresponding to $\mu_B \approx 0.406$ GeV and $\sqrt{s} \approx 9.3$ GeV which are almost exactly the values for T_{ch} and μ_B the present work gets.

It is noteworthy that the kinetic freeze-out temperature for the emission of multi-strange particles is observed considerably higher than those for the emissions of other identified particles, which reveals a picture of separate freeze-out processes for other identified and multi-strange particles. Meanwhile, the transverse flow velocity of multi-strange particles is lower than that of other identified particles. The reason behind the high kinetic freeze-out temperature (low transverse flow velocity) may be that the multi-strange hadrons can be left behind in the system evolution process due to their large mass. This possibility is a reflection of hydrodynamic behavior [100], in which massive particles are leaved due to their small velocity.

With the increase of collision energy, both the kinetic freeze-out temperature T_0 and transverse flow velocity β_T increase or keep invariant if phase transition had happened in part volume. There is a positive correlation between T_0 and β_T when we study them over a

wide energy range. This renders that the system stays at high excitation state and undergoes large squeeze and expansion due to large energy deposition at high energy. This work does not support the negative correlation between T_0 and β_T when we increase the energy, though negative correlation can be explained as long lifetime (then low excitation) and large squeeze and expansion. Deservedly, for a given spectrum, T_0 and β_T is negative correlation, which is not the case for varying energy.

The values of q extracted from the spectra of π^+ , K^+ , p , K_S^0 , ϕ , Λ , $\bar{\Xi}^+$ (Ξ^+ , Ξ) and $\bar{\Omega}^+$ ($\Omega^- + \Omega^+$, Ω) in central AA collisions at different energies do not show particular behavior, but hardly energy dependent or slightly change with energy. As an entropy index, q characterizes the degree of equilibrium of the system. Generally, an equilibrium state corresponds to q to be 1. The values of q obtained in this work are approximately close to 1, which renders that the system in the considered energy range stays approximately in an equilibrium state or in a few local equilibrium states. This also renders that the blast-wave fit is approximately useable in this work.

However, it should be noted that the entropy index q is a very very sensitive quantity. A large q which is not close to 1 results in a wide distribution, and a small q which is close to 1 results in a narrow distribution. It is the fact that $q = 1.01$ is not close enough to 1. So, it does not imply that the Tsallis blast-wave fit is close to its Boltzmann-Gibbs counterpart if we use the same T_0 and β_T in the case of $q = 1.01$. To reduce the difference between the Tsallis blast-wave fit and its Boltzmann-Gibbs counterpart, we need $q = 1.0001$ or the one which is closer to 1.

4 Summary and conclusions

The main observations and conclusions are summarized here.

(a) The transverse momentum (mass) spectra of π^+ , K^+ , p , K_S^0 , ϕ , Λ , $\bar{\Xi}^+$ (Ξ^+ , Ξ) and $\bar{\Omega}^+$ ($\Omega^- + \Omega^+$, Ω) produced in central AA collisions at mid- y or mid- η over an energy range from 2.7 GeV to 2.76 TeV have been studied by the blast-wave fit with Tsallis statistics. The kinetic freeze-out temperature T_0 and transverse flow velocity β_T are extracted from the fit to transverse momentum (mass) spectra.

(b) The excitation functions of T_0 and β_T show that both T_0 and β_T increase sharply with the increase of col-

lision energy from 2.7 to 7.7 GeV. Then they remains invariant from 7.7 to 39 GeV. At above 39 GeV, they show the trend of increase. The three energy ranges have identifiable boundaries and render three different interaction mechanisms or evolution processes.

(c) The system is baryon-dominated from 2.7 to 7.7 GeV, in which there is no phase transition from hadron matter to QGP due to low energy deposition. The system starts its phase transition in part volume at 7.7 GeV and undergoes from baryon-dominated to meson-dominated due to phase transition in larger and larger volume in 7.7–39 GeV. The system is meson-dominated at above 39 GeV, in which the phase transition had happened in whole volume.

(d) The onset energy of part phase transition from hadron matter to QGP is 7.7 GeV and that of whole phase transition is 39 GeV. The multi-strange and other identified particles shows separate freeze-out process due to the difference in temperature and flow velocity. From the refined structure, the multiple freeze-out scenarios are also observed due to the mass dependent temperature and flow velocity.

Data availability

The data used to support the findings of this study are included within the article and are cited at relevant places within the text as references.

Ethical approval

The authors declare that they are in compliance with ethical standards regarding the content of this paper.

Disclosure

The funding agencies have no role in the design of the study; in the collection, analysis, or interpretation of the data; in the writing of the manuscript; or in the decision to publish the results.

Conflict of interest

The authors declare that there are no conflicts of interest regarding the publication of this paper.

Acknowledgments

This work was supported by the National Natural Science Foundation of China under Grant Nos.

11575103, 11947418, and 11505104, the Chinese Government Scholarship (China Scholarship Council), the Scientific and Technological Innovation Programs of Higher Education Institutions in Shanxi (STIP) under Grant No. 201802017, the Shanxi Provincial Natural Science Foundation under Grant No. 201901D111043, and the Fund for Shanxi “1331 Project” Key Subjects Construction.

References

- [1] BRAHMS Collaboration (I. Arsene *et al.*), Nucl. Phys. A **757**, 1 (2005).
- [2] PHENIX Collaboration (K. Adcox *et al.*), Nucl. Phys. A **757**, 184 (2005).
- [3] PHOBOS Collaboration (B.B. Back *et al.*), Nucl. Phys. A **757**, 28 (2005).
- [4] STAR Collaboration (J. Adams *et al.*), Nucl. Phys. A **757**, 102 (2005).
- [5] J. Cleymans, K. Redlich, Phys. Rev. C **60**, 054908 (1999).
- [6] F. Becattini, J. Manninen, M. Gazdzicki, Phys. Rev. C **73**, 044905 (2006).
- [7] A. Andronic, P. Braun-Munzinger, J. Stachel, Nucl. Phys. A **772**, 167 (2006).
- [8] E. Laermann, O. Philipsen, Ann. Rev. Nucl. Part. Sci. **53**, 163 (2003).
- [9] Y. Aoki, G. Endrodi, Z. Fodor, S. D. Katz, K.K. Szabo, Nature **443**, 675 (2006).
- [10] M. Cheng, N.H. Christ, S. Datta, J. van der Heide, C. Jung, F. Karsch, O. Kaczmarek, E. Laermann, R.D. Mawhinney, C. Miao, P. Petreczky, K. Petrov, C. Schmidt, W. Soeldner, T. Umeda, Phys. Rev. D **77**, 014511 (2008).
- [11] M. Asakawa, K. Yazaki, Nucl. Phys. A **504**, 668 (1989).
- [12] A. Barducci, R. Casalbuoni, S. De Curtis, R. Gatto, G. Pettini, Phys. Rev. D **41**, 1610 (1990).
- [13] M.A. Stephanov, Prog. Theor. Phys. Suppl. **153**, 139 (2004).
- [14] M.A. Stephanov, Int. J. Mod. Phys. A **20**, 4387 (2005).
- [15] Z. Fodor, S.D. Katz, JHEP **0404**, 050 (2004).
- [16] R.V. Gavai, S. Gupta, Phys. Rev. D **78**, 114503 (2008).
- [17] S. Rao, M. Sievert, J. Noronha-Hostler, arXiv:1910.03677 [nucl-th] (2019).
- [18] G. Odyniec for the STAR Collaboration, PoS **CORFU2018**, 151 (2018).
- [19] M. Tokarev, A. Kechechyan, I. Zborovský, Nucl. Phys. A **993**, 121646 (2020).
- [20] L. Kumar for the STAR Collaboration, Nucl. Phys. A **904–905**, 256c (2013).
- [21] L. Kumar, Mod. Phys. Lett. A **28**, 1330033 (2013).
- [22] U. Heinz, J. Phys. G **25**, 263 (1999).
- [23] M. Waqas, B.-C. Li, Adv. High Energy Phys. **2020**, 1787183 (2020).
- [24] M. Waqas, F.-H. Liu, Eur. Phys. J. Plus **135**, 147 (2020).
- [25] H.-L. Lao, F.-H. Liu, B.-C. Li, M.-Y. Duan, R. A. Lacey, Nucl. Sci. Tech. **29**, 164 (2018).
- [26] H.-L. Lao, F.-H. Liu, B.-C. Li, M.-Y. Duan, Nucl. Sci. Tech. **29**, 82 (2018).
- [27] Z.B. Tang, Y.C. Xu, L.J. Ruan, G. van Buren, F.Q. Wang, Z.B. Xu, Phys. Rev. C **79**, 051901(R) (2009).
- [28] S. Chatterjee, S. Das, L. Kumar, D. Mishra, B. Mohanty, R. Sahoo, N. Sharma, Adv. High Energy Phys. **2015**, 349013 (2015).
- [29] S. Chatterjee, B. Mohanty, R. Singh, Phys. Rev. C **92**, 024917 (2015).
- [30] S. Chatterjee, B. Mohanty, Phys. Rev. C **90**, 034908 (2014).
- [31] D. Thakur, S. Tripathy, P. Garg, R. Sahoo, J. Cleymans, Adv. High Energy Phys. **2016**, 4149352 (2016).
- [32] F.-H. Liu, Y.-Q. Gao, T. Tian, B.-C. Li, Eur. Phys. J. A **50**, 94 (2014).
- [33] P.Z. Ning, L. Li, D.F. Min, Foundation of Nuclear Physics: Nucleons and Nuclei (Higher Education Press, Beijing, China, 2003).
- [34] H.-L. Lao, H.-R. Wei, F.-H. Liu, R. A. Lacey, Eur. Phys. J. A **52**, 203 (2016).
- [35] T. S. Biró, G. Purcsel and K. Ürmössy, Eur. Phys. J. A **40**, 325 (2009).
- [36] J. Cleymans, D. Worku, Eur. Phys. J. A **48**, 160 (2012).
- [37] G.G. Barnaföldi, K. Ürmössy, T. S. Biró, J. Phys. Conf. Ser. **270**, 012008 (2011).
- [38] J.C. Chen, Z.P. Zhang, G.Z. Su, L.X. Chen, Y.G. Shu, Phys. Lett. A **300**, 65 (2002).
- [39] J.M. Conroy, H.G. Miller, Phys. Rev. D **78**, 054010 (2008).
- [40] G. Biró, G.G. Barnaföldi, T.S. Biró, K. Ürmössy, AIP Conf. Proc. **1853**, 080001 (2017).
- [41] A.M. Teweldeberhan, A.R. Plastino, H.G. Miller, Phys. Lett. A **343**, 71 (2004).
- [42] J.M. Conroy, H.G. Miller, A.R. Plastino, Phys. Lett. A **374**, 4581 (2010).
- [43] F.M. Ciaglia, A. Ibort, G. Marmo, Int. J. Geom. Meth. Mod. Phys. **16**, 1950136 (2019).
- [44] R.C. Wang, C.Y. Wong, Phys. Rev. D **38**, 348 (1988).
- [45] M. Waqas, F.-H. Liu, S. Fakhraddin, M.A. Rahim, Indian J. Phys. **93**, 1329 (2019).
- [46] E. Schnedermann, J. Sollfrank, U. W. Heinz, Phys. Rev. C **48**, 2462 (1993).
- [47] STAR Collaboration (B.I. Abelev *et al.*), Phys. Rev. C **79**, 034909 (2009).
- [48] A. Khuntia, H. Sharma, S. Kumar Tiwari, R. Sahoo, J. Cleymans, Eur. Phys. J. A **55**, 3 (2019).

- [49] CMS Collaboration (S. Chatrchyan *et al.*), Eur. Phys. J. C **72**, 1945 (2012).
- [50] M. Suleymanov, Int. J. Mod. Phys. E **27**, 1850008 (2018).
- [51] E.K.G. Sarkisyan, A.S. Sakharov, AIP Conf. Proc. **828**, 35 (2006).
- [52] E.K.G. Sarkisyan, A.S. Sakharov, Eur. Phys. J. C **70**, 533 (2010).
- [53] A.N. Mishra, R. Sahoo, E.K.G. Sarkisyan, A.S. Sakharov, Eur. Phys. J. C **74**, 3147 (2014).
- [54] E.K.G. Sarkisyan, A.N. Mishra, R. Sahoo, A.S. Sakharov, Phys. Rev. D **93**, 054046 (2016).
- [55] E.K.G. Sarkisyan, A.N. Mishra, R. Sahoo, A.S. Sakharov, Phys. Rev. D **94**, 011501 (2016).
- [56] E.K.G. Sarkisyan, A.N. Mishra, R. Sahoo, A.S. Sakharov, EPL **127**, 62001 (2019).
- [57] A.N. Mishra, A. Ortiz, G. Paić, Phys. Rev. C **99**, 034911 (2019).
- [58] P. Castorina, A. Iorio, D. Lanteri, H. Satz, M. Spousta, Phys. Rev. C **101**, 054902 (2020).
- [59] M. D. Azmi, J. Cleymans, Eur. Phys. J. C **75**, 430 (2015).
- [60] F.-H. Liu, Y.-Q. Gao, H.-R. Wei, Adv. High Energy Phys. **2014**, 293873 (2014).
- [61] K. Jiang, Y.Y. Zhu, W.T. Liu, H.F. Chen, C. Li, L.J. Ruan, Z.B. Tang, Z.B. Xu, Phys. Rev. C **91**, 024910 (2015).
- [62] A. S. Parvan, T. Bhattacharyya, Eur. Phys. J. A **56**, 72 (2020).
- [63] R. Hagedorn, Riv. Nuovo Cimento, **6**(10), 1 (1983).
- [64] ALICE Collaboration (B.B. Abelev *et al.*), Eur. Phys. J. C **75**, 1 (2015).
- [65] R. Odorico, Phys. Lett. B **118**, 151 (1982).
- [66] UA1 Collaboration (G. Arnison *et al.*), Phys. Lett. B **118**, 167 (1982).
- [67] M. Biyajima, T. Mizoguchi, N. Suzuki, Int. J. Mod. Phys. A **32**, 1750057 (2017).
- [68] E866 and E917 Collaborations (L. Ahle *et al.*), Phys. Lett. B **476**, 1 (2000).
- [69] E895 Collaboration (J.L. Klay *et al.*), Phys. Rev. Lett. **88**, 102301 (2002).
- [70] E895 Collaboration (J.L. Klay *et al.*), Phys. Rev. C **68**, 054905 (2003).
- [71] E802 Collaboration (L. Ahle *et al.*), Phys. Rev. C **58**, 3523 (1998).
- [72] E802 Collaboration (L. Ahle *et al.*), Phys. Rev. C **57**, R466(R) (1998).
- [73] STAR Collaboration (L. Adamczyk *et al.*), Phys. Rev. C **96**, 044904 (2017).
- [74] V. Bairathi for the STAR Collaboration, Nucl. Phys. A **956**, 292 (2016).
- [75] M. Shao for the STAR Collaboration, J. Phys. G **31**, S85 (2005).
- [76] PHENIX Collaboration (K. Adcox *et al.*), Phys. Rev. Lett. **88**, 242301 (2002).
- [77] PHENIX Collaboration (S. S. Adler *et al.*), Phys. Rev. C **69**, 034909 (2004).
- [78] ALICE Collaboration (B. Abelev *et al.*), Phys. Rev. C **88**, 044910 (2013).
- [79] HADES Collaboration (G. Agakishiev *et al.*), Phys. Rev. C **82**, 044907 (2010).
- [80] HADES Collaboration (J. Adamczewski *et al.*), Phys. Lett. B **793**, 457 (2019).
- [81] STAR Collaboration (J. Adam *et al.*), arXiv:1906.03732 (2019).
- [82] STAR Collaboration (M.M. Aggarwal *et al.*), Phys. Rev. C **83**, 024901 (2011).
- [83] STAR Collaboration (C. Adler *et al.*), Phys. Lett. B **595**, 143 (2004).
- [84] CMS Collaboration (V. Khachatryan *et al.*), Phys. Lett. B **768**, 103 (2017).
- [85] STAR Collaboration (B.I. Abelev *et al.*), Phys. Rev. C **79**, 064903 (2009).
- [86] ALICE Collaboration (B.I. Abelev *et al.*), Phys. Lett. B **595**, 143 (2004).
- [87] FOPI Collaboration (M. Merschmeyer *et al.*), Phys. Rev. C **76**, 024906, (2007).
- [88] S. Uddin, R.A. Bhat, I.-U. Bashir, arXiv:1412.2663 (2014).
- [89] V. Begun, W. Florkowski, M. Rybczynski, Phys. Rev. C **90**, 054912 (2014).
- [90] NA49 Collaboration (N.G. Antoniou *et al.*), Phys. Rev. C **81**, 064907 (2010).
- [91] NA49 Collaboration (T. Anticic *et al.*), Phys. Rev. C **94**, 044906 (2016).
- [92] M. Maćkowiak-Pawłowska for the NA61/SHINE and NA49 Collaborations, arXiv:1212.6880 (2012).
- [93] K. Grebieszko for the NA49 and NA61/SHINE Collaborations, PoS **EPS-HEP2009**, 030 (2009).
- [94] NA61/SHINE Collaboration (N. Abgrall *et al.*), Eur. Phys. J. C **79**, 100 (2019).
- [95] V. Klochov and I. Selyuzhenkov for the NA61/SHINE Collaboration, Nucl. Phys. A **982**, 439 (2019).
- [96] J. Cleymans, H. Oeschler, K. Redlich, S. Wheaton, Phys. Rev. C **73**, 034905 (2006).
- [97] A. Andronic, P. Braun-Munzinger, J. Stachel, Nucl. Phys. A **834**, 237c (2010).
- [98] A. Andronic, P. Braun-Munzinger, K. Redlich, J. Stachel, Nature **561**, 321 (2018).
- [99] M.A. Stankiewicz, arXiv:nucl-th/0509058 (2005).
- [100] R. Sahoo, AAPS Bulletin, **29**(4), 16 (2019).